SCIENTIFIC REPORTS

OPEN

Fate of Barium Sulfate Nanoparticles Deposited in the Lungs of Rats

Received: 29 November 2018
Accepted: 20 May 2019
Published online: 03 June 2019

Ramon M. Molina[1], Nagarjun V. Konduru[1], Priscila M. Queiroz[1], Benjamin Figueroa[2], Dan Fu[2], Lan Ma-Hock[3], Sibylle Groeters[3], Dirk Schaudien[4] & Joseph D. Brain[1]

We have shown that barium [from $BaSO_4$ nanoparticles (NPs)] was cleared from the lungs faster than other poorly soluble NPs and translocated mostly to bone. We now studied barium biokinetics in rats during Study 1: two-year inhalation exposure to 50 mg/m^3 $BaSO_4$ NP aerosols, and Study 2: single intratracheal (IT) instillation of increasing doses of $BaSO_4$ NPs or $BaCl_2$. Study 1 showed that lung barium content measured by inductively coupled plasma mass spectrometry increased during 360 days of $BaSO_4$ NP aerosol exposures. An equilibrium was established from that time until 2 years. Barium concentrations in $BaSO_4$-exposed animals were in the order (lungs > lymph nodes > hard bone > bone marrow > liver). In Study 2, there was an increase in lung barium post-IT instillation of $BaSO_4$ NPs while barium from $BaCl_2$ was mostly cleared by day 28. Transmission electron microscopy showed intact $BaSO_4$ NPs in alveolar macrophages and type II epithelial cells, and in tracheobronchial lymph nodes. Using stimulated Raman scattering microscopy, specific $BaSO_4$ Raman spectra were detected in $BaSO_4$ NP-instilled lungs and not in other organs. Thus, we posit that barium from $BaSO_4$ NPs translocates from the lungs mainly after dissolution. Barium ions are then incorporated mostly into the bone and other organs.

Barium sulfate particles are usually included in the family of poorly soluble particles (PSP) or poorly soluble low toxicity (PSLT) particles. These categories also include cerium dioxide (CeO_2) and titanium dioxide (TiO_2)[1–3]. These so-called biodurable nanomaterials are thought to be poorly absorbed into the blood from the gut or lungs[4–6]. Determining the fate of $BaSO_4$ NPs is important because they have extensive commercial applications. Barium sulfate nanoparticles ($BaSO_4$ NPs) are used as fillers in coatings (e.g., in motor vehicles), in orthopedic medicine, diagnostic imaging and other applications[7–10]. It has been reported that pellethane, a polyurethane elastomer, when incorporated with $BaSO_4$ NPs exhibits antimicrobial properties *in vitro*[11].

The toxicity and biokinetics of nanoparticles are influenced by their physicochemical properties[12–16]. Poorly soluble particles usually have slower clearance kinetics and diminished biological effects compared to soluble particles[3,17,18]. For example, CeO_2 and far more soluble ZnO NPs of similar size were cleared at vastly different rates from the lungs. Rapidly dissolving ZnO NPs elicited more acute pulmonary inflammation, and disappeared much faster that CeO_2 NPs[19,20]. We have shown that $BaSO_4$ NPs instilled into the lungs of rats elicited less injury and inflammation than do CeO_2 NPs of similar primary NP size and amount[18,20]. Finally, particles of different sizes with the same composition elicit different biological responses[21–23]. Dissolution rates and biologic responses increase as particle size decreases at the same mass dose. Moreover, the lung clearance of radioactive barium after intratracheal (IT) instillation of $^{131}BaSO_4$ was influenced by particle size[24,25]. These two studies produced retention half-lives of radioactive 1.45 µm and 3.6 µm $^{133}BaSO_4$ particles of approximately 2 and 10 days, respectively. Higher initial lung burden of the larger particles also increased the half-life from 10 to 27 days[25].

To explore the relative toxicity of $BaSO_4$ (NM-220) and CeO_2 (NM-212) NPs for manufacturers as well as consumers, a long-term project was funded by the German Federal Ministry of Education and Research. This project is managed within the Organization for Economic Cooperation and Development (OECD) and the European

[1]Molecular and Integrative Physiological Sciences Program, Department of Environmental Health, Harvard T.H. Chan School of Public Health, 665 Huntington Avenue, Boston, MA, 02115, USA. [2]Department of Chemistry, University of Washington, 36 Bagley Hall, Seattle, WA, 98195, USA. [3]BASF SE, Carl-Bosch-Straße 38, 67056, Ludwigshafen, Germany. [4]Fraunhofer-Institute for Toxicology and Experimental Medicine ITEM Nikolai-Fuchs-Str. 1, 30625, Hannover, Germany. Correspondence and requests for materials should be addressed to R.M.M. (email: rmolina@hsph.harvard.edu)

Duration of Exposure	Targeted concentrations (mg/m^3)	Measured concentrations (mg/m^3)	MMAD/ GSD mean (μm)	Particle count concentration ($particle/cm^3$)	Particle count median diameter (nm)
2 years	50	50.3 ± 5.8	2.0/2.0	45,900	341

Table 1. Aerosol concentrations and particle size distributions of $BaSO_4$ NM-220. Based on 16 measurements (10 replicates) over the two-year period. Data are mean ± SD.

Union Project NANoREG (a Europe-wide approach to the regulatory testing of manufactured nanomaterials). An inhalation study in rats and associated analytic procedures were conducted at BASF SE, Experimental Toxicology and Ecology Ludwigshafen, Germany. The NM-220 and NM-212 used in this project are well characterized nanomaterials from the European Commission Joint Research Center (JRC) nanomaterial (NM) repository (Ispra, Italy). Both CeO_2 (NM-212) and $BaSO_4$ (NM-220) have low water solubility[18,20]. In the earlier phase of this project, we found that despite the reported low solubility of $BaSO_4$ NPs, barium was cleared from the lungs much more rapidly compared to other poorly soluble nanoparticles, including CeO_2[3,18,20]. Since it was established in short-term inhalation studies that $BaSO_4$ does not cause adverse health effects[26–28] at the doses studied, a concentration of 50 mg/m^3 was selected by BASF SE for the 2-year repeated inhalation exposures, a level at which lung overload might be expected.

We recently showed that lung clearance of ^{131}Ba post-instillation of $^{131}BaSO_4$ NPs was significantly faster than of ^{141}Ce post-instillation of $^{141}CeO_2$ NPs at the same mass dose in the same male rat strain and age[18,20]. Interestingly, we found that the major sites of retention of barium translocated from the lungs were bone, bone marrow, and tracheobronchial and mediastinal lymph nodes. These biokinetic data were based on tissue ^{131}Ba (radioactivity) or Ba measurements by inductively coupled plasma-mass spectrometry (ICP-MS). Neither method could differentiate whether the measured barium was present in intact $BaSO_4$ NPs, ionic barium or new structural forms containing Ba.

The aims of our research are: Study 1 to measure retention of barium in multiple organs of rats that inhaled $BaSO_4$ NPs during the 2-year inhalation exposure described earlier and Study 2 to examine the role of $BaSO_4$ particle dissolution in the translocation of barium from the lungs to extra-pulmonary tissues especially the bone and lymph nodes. A common goal in both studies is to characterize the chemical form and morphology of retained barium in the lungs, bone, and tracheobronchial lymph nodes. To pursue the first aim, we measured barium concentrations in the lungs and selected organs in rats from the 2-year inhalation study at BASF SE. In the second aim, we compared lung and bone concentrations of barium in rats IT-instilled with $BaSO_4$ NPs versus $BaCl_2$ solution. Finally, we used electron microscopy and stimulated Raman Scattering (SRS) microscopy to provide qualitative insights into the chemical form of barium in the lungs and other tissues. Our overall goal was to explore the mechanisms of clearance of $BaSO_4$ NPs from the lungs and to quantify and understand the mechanisms for the retention of barium in extrapulmonary organs.

Results

Study 1: Long-term inhalation exposure to $BaSO_4$ aerosols. *Biokinetics of inhaled $BaSO_4$ NPs.* A complete physicochemical characterizations of $BaSO_4$ NPs (NM-220) has been reported[18,28]. Selected physicochemical endpoints for NM-220 and the similar reproduced $BaSO_4$ NPs used in Study 1 are summarized in Table S1 (Supplement). For the long-term inhalation study, the particle concentrations and size distribution of generated $BaSO_4$ aerosols are summarized in Table 1. The target concentration of about 50 mg/m^3 was maintained throughout the inhalation exposures. The particle size distribution of aerosolized $BaSO_4$ NP aggregates had an approximate MMAD of 2.0 μm and thus was in the respirable range for rats.

After the final day of the multiple inhalation exposure of rats for 2 years, four $BaSO_4$ aerosol-exposed and two filtered air-exposed controls were euthanized, and samples were sent to Harvard for further analyses. The barium concentrations and estimated total barium in the lungs, liver, lymph nodes, bone and bone marrow were measured. Based on these current data obtained at 2 years and on the previous reports in rats examined at 1, 28, and 90 days[18,28], we constructed a cumulative lung retention curve over the two-year period (Fig. 1A). The combined data showed that barium accumulated in the lungs with time up to 360 days. An equilibrium was established from that point until 730 days. During that period, deposition rate equaled clearance rate. Tissue concentrations and total amounts of barium in the lungs, bone (without marrow), bone marrow, liver and lymph nodes are shown in Table 2. Detectable amounts of barium in these organs were also present in air-exposed control rats almost certainly from background air borne and dietary sources. In both air-exposed controls and $BaSO_4$-exposed rats, barium concentrations significantly differed among the organs we examined (ANOVA, $P = 0.04$). Additionally, significantly greater barium was found in the lungs ($P = 0.003$) and bones ($P = 0.038$) of $BaSO_4$-exposed than in air-exposed controls. The highest barium concentrations in the $BaSO_4$-exposed animals were measured in the lungs and lymph nodes (tracheobronchial and mediastinal), followed by the hard bone and bone marrow, while the liver had the lowest concentration. The total lung and liver barium contents were based on actual organ weights while those for bone and bone marrow were computed using estimates of their tissue percentage of total body weight: 3.2% bone marrow and 5% bone[29]. The highest amounts of barium from the exposed animals were found in the lungs as expected, and in hard bone. Based on reported lung barium data from the same 2-year inhalation study (Study 1)[28], we generated a lung clearance curve for barium after multiple inhalation exposures over 90 days (Fig. 1B). The total lung barium and concentration at day 90 were 1.60 mg/lung and 1.24 mg/g, respectively. The clearance half-time from that time point onward was approximately 56 days. Since rats were unavailable after the end of the inhalation exposure, lung clearance when retained barium is higher could not be determined.

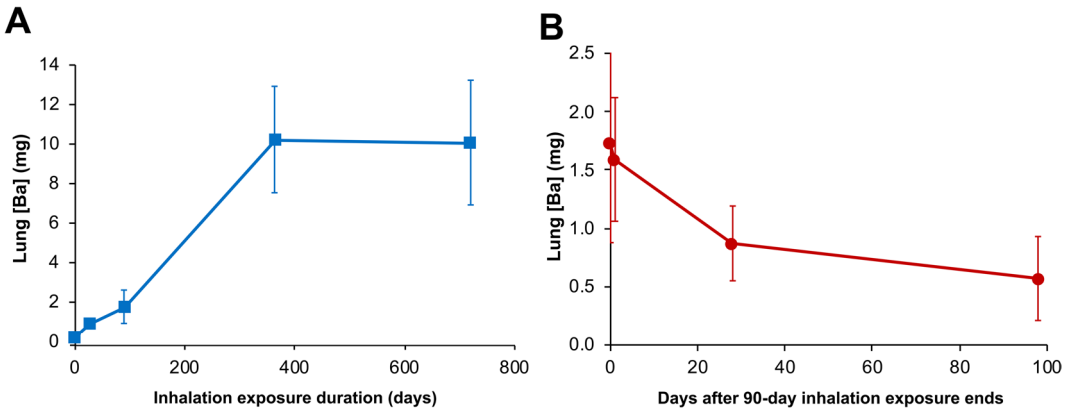

Figure 1. Study 1. (**A**) Cumulative retention of barium in the lungs of rats during inhalation exposures to 50 mg/m^3 $BaSO_4$ NPs aerosols or filtered air. Lung burdens of barium in $BaSO_4$ NPs aerosol exposed rats examined at 1, 28, 90, 364 and 730 days and air-exposed rats at 730 days. Air-exposed rat lungs had only 0.04 ± 0.01 µg barium. (**B**) Clearance of retained barium after 90-day multiple inhalation exposures to 50 mg/m^3 barium sulfate nanoparticles. The retained barium at 90 days was 1.6 mg/lung (1.24 mg/g lung). The clearance half-time after 90 days exposure was approximately 56 days. This clearance graph was based on data from reference[28].

	Filtered Air			$BaSO_4$		
Study 1	[Ba] µg/g	Organ Wt. (g)	Total Ba (µg)	[Ba] µg/g	Organ Wt. (g)	Total Ba (µg)
Lungs	0.04 ± 0.01$^{\#}$	1.11 ± 0.12	0.04 ± 0.01$^{\#}$	5808 ± 2552$^{\#,*}$	1.91 ± 0.78	10056 ± 3148$^{\#}$
Bone	7.33 ± 0.62	18.35 ± 0.29	134.6 ± 13.4	348 ± 70.1*	15.90 ± 1.34	5546 ± 1348
Bone Marrow	6.24 ± 4.58	11.74 ± 0.19	72.8 ± 52.7	73.2 ± 109	10.18 ± 0.86	781 ± 1199
Liver	0.04 ± 0.03	11.22 ± 0.22	0.40 ± 0.31	0.12 ± 0.05	9.41 ± 0.63	1.06 ± 0.39
Lymph Nodes	7.48 ± 1.82	N.D.	N.D.	4461 ± 3492	N.D.	N.D.

Table 2. Barium concentration and content in the lungs and selected organs of rats after chronic exposures to 50 mg/m^3 $BaSO_4$ NPs or filtered air (6 h/day, 5 consecutive days/week) for 2 years. Data are mean ± SD, n = 2 filtered air-exposed control, n = 4 $BaSO_4$ NP-exposed rats. Barium concentration in tracheobronchial and mesenteric lymph nodes were pooled. Bone and bone marrow weights were estimated as 5% and 3.2% of body weight, respectively. N.D., not determined, estimate of total lymph node mass in rats is not available. *$P < 0.05$, Student's T test, air-exposed vs. $BaSO_4$-exposed. $^{\#}P < 0.05$, ANOVA, significant differences among organs.

Transmission electron microscopic examination of tissues from rats in Study 1. The distribution of retained $BaSO_4$ NPs in the lungs of rats was examined by transmission electron microscopy. Figure 2 shows a rat lung one day after the final inhalation exposure to 50 mg/m^3 $BaSO_4$ NPs aerosols that lasted for two years. The majority of the particles were seen within phagolysosomes in alveolar macrophages (Fig. 2A,B). $BaSO_4$ NPs were occasionally observed in type II epithelial cells (Fig. 2C,D). The majority of observed $BaSO_4$ NPs were seen within phagolysosomes in macrophages and occasionally in neutrophils (data not shown). Since barium concentrations in both tracheobronchial and mesenteric lymph nodes were nearly as high as in the lungs, ultrastructural examination with TEM was also performed. We observed $BaSO_4$ NPs within endosomes of phagocytic cells in tracheobronchial lymph nodes (Fig. 3). No evidence of particles was seen in the mesenteric lymph nodes despite the presence of a high concentration of barium measured by ICP-MS. No evidence of particles was seen in the bone marrow, the liver or the lungs of air-exposed controls.

Study 2: Intratracheal instillation of $BaSO_4$ nanoparticles versus soluble $BaCl_2$ in rats. *Biokinetics of IT- instilled $BaSO_4$ nanoparticles versus soluble $BaCl_2$.* Characterization of $BaSO_4$ NP (NM-220 batch) suspensions used in Study 2 is summarized in Table 3. The agglomerate sizes were assessed using dynamic light scattering (DLS). We found that the agglomerate sizes were influenced by particle concentration: the higher the concentration, the larger the hydrodynamic diameter (Table 3, Fig. 4). The most concentrated 33.3 mg/ml suspension showed a bimodal distribution indicating the presence of two distinct populations of different sized particle agglomerates. Transmission electron micrographs of $BaSO_4$ NPs suspended in distilled water show a non-spherical globular shape of individual nanoparticles (Fig. 5). They appeared as individual particles or as agglomerates of variable sizes that roughly corresponded to the range of hydrodynamic sizes obtained by DLS. The zeta potentials were all negative and decreased in magnitude in the most concentrated suspension (from −18 mV to −10 mV).

To determine the contribution of NP dissolution in the biokinetics of barium post-instillation of $BaSO_4$ NPs, we measured barium concentrations in the lungs and bones of rats instilled with increasing doses of $BaSO_4$ NPs versus dissolved $BaCl_2$ at 28 days post-instillation (Fig. 6, Table 4). First, there were significant increases in lung

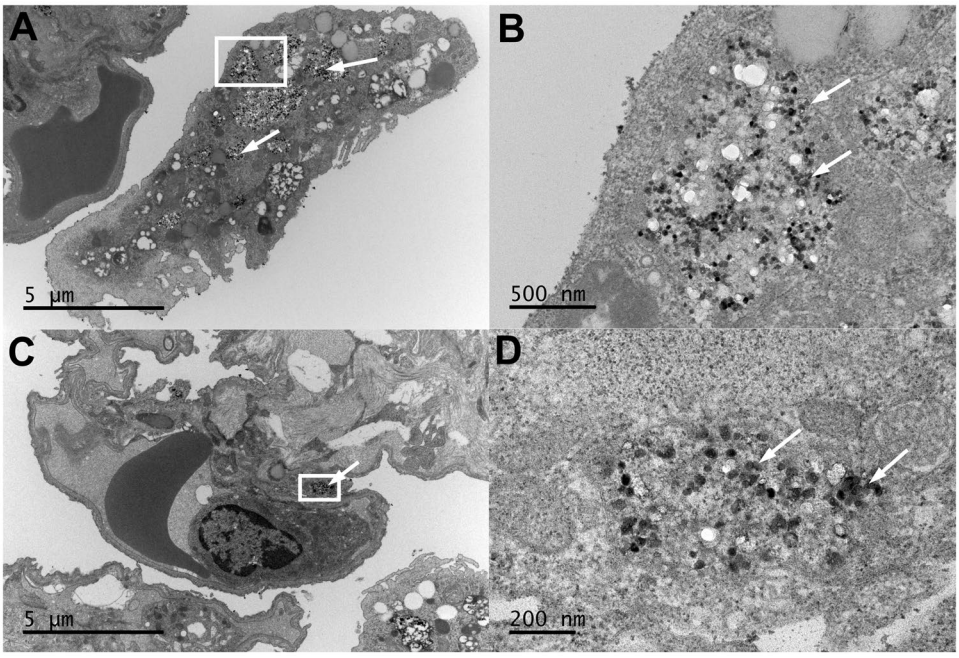

Figure 2. Study 1. Rat lung after 24 months of multiple inhalation exposures to 50 mg/m^3 $BaSO_4$ NPs aerosols. (**A**) An alveolar macrophage with engulfed $BaSO_4$ nanoparticles (arrows) within phagolysosomes. (**B**) Higher magnification of boxed area in panel A showing $BaSO_4$ particles (arrows). (**C**) Type II epithelial cell with internalized $BaSO_4$ nanoparticles (arrows). (**D**) Higher magnification of boxed area in panel C showing $BaSO_4$ particles (arrows) within a type 2 epithelial cell.

retention up to the 10 mg/kg dose. However, at the higher dose of 50 mg/kg, the amount of barium retained in the lungs did not increase, indicating faster clearance rates (Table 4, Fig. 6). Barium in ionic form ($BaCl_2$) even at 10 mg/kg dose was mostly cleared by day 28. At 10 mg/kg dose, the lung barium concentration in the $BaCl_2$ group was 20 µg/g compared to 285 µg/g from the $BaSO_4$ NP group. In contrast with the lungs, significantly higher amounts of barium were retained in the bones of rats instilled with $BaCl_2$ compared to rats administered with $BaSO_4$ NPs (Fig. 6B). The bone and lymph node barium concentrations significantly increased with increasing dose of both $BaSO_4$ NPs and $BaCl_2$ (ANOVA, $P < 0.001$). The slopes of bone and lymph node barium concentrations between $BaCl_2$ and $BaSO_4$ animals were also significantly different (ANOVA, $P < 0.001$) (Table 4).

Transmission electron microscopic examination of lungs and other tissues in Study 2. The cellular/tissue localization of retained $BaSO_4$ NPs in the lungs of rats was examined by transmission electron microscopy. Figure 7 shows a rat lung immediately after and at 7 days post-IT instillation with 1 mg/kg $BaSO_4$ nanoparticles. When we examined the rat lungs about 5 minutes after instillation, the majority of instilled particles were seen extracellularly in the alveoli interspersed within alveolar lining materials. Later at 7 days, the majority of $BaSO_4$ NPs were seen within phagolysosomes in alveolar macrophages (Fig. 7C,D) and occasionally in type II epithelial cells (Fig. 7E,F). The $BaSO_4$ NPs were densely packed within phagolysosomes and had a similar appearance to the original particle suspension delivered to the lungs (Fig. 5). In contrast, the $BaSO_4$ particles inside the alveolar macrophages after 2 years of chronic inhalation were sparsely distributed and were interspersed with electron lucent materials (Fig. 2B). Individual particles were less electron dense and lacked the typical globular shape of the original NPs suggesting gradual dissolution.

Stimulated Raman Scattering microscopy of lungs and other tissues from IT-instilled rats. To determine if $BaSO_4$ NPs translocate to the bone as intact particles or as ionic barium, additional spectroscopic analysis of tissue samples from Study 2 were performed with SRS microscopy. This technique is based on identifying the characteristic Raman shifts of $BaSO_4$ in unstained tissue sections. The lung, bone, liver, spleen and kidney of rats instilled with $BaSO_4$ NPs or soluble $BaCl_2$ were examined at 28 days post-instillation. Our results show that the signature Raman shift of $BaSO_4$ was present in several foci in the lungs of rats instilled with $BaSO_4$ NPs (Fig. 8A,B) but not with ionic $BaCl_2$ (Fig. 8C,D). No signature Raman shift for $BaSO_4$ was found in the control (uninstilled) lung (data not shown) nor in bone (Fig. 8E,F) of rats instilled with $BaSO_4$ NPs or soluble $BaCl_2$. No spectral signature of $BaSO_4$ was detected in the liver, spleen and kidneys from control (uninstilled) and from $BaCl_2$- and $BaSO_4$-instilled rats (data not shown).

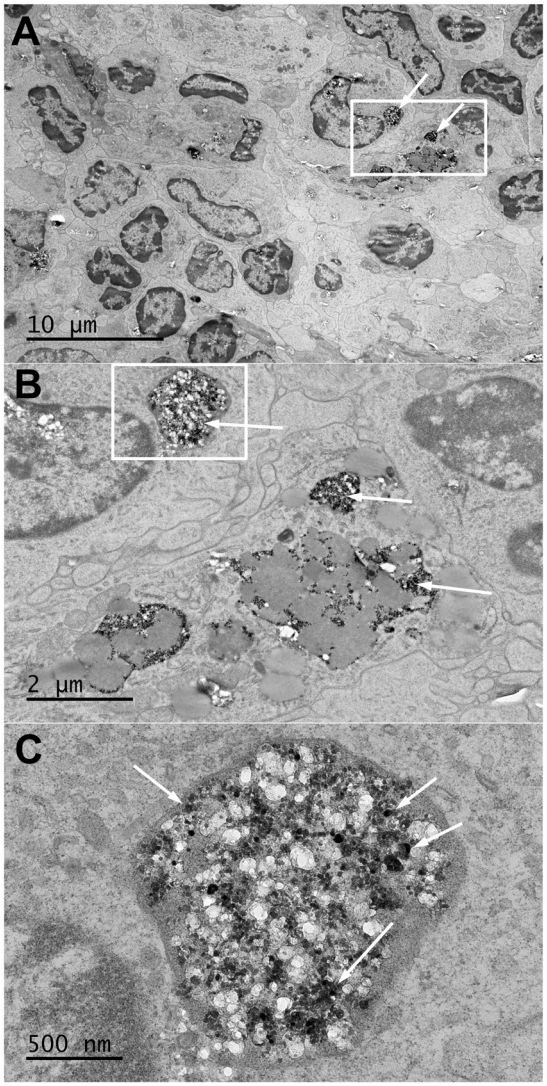

Figure 3. Study 1. Rat tracheobronchial lymph node after 24 months of multiple inhalation exposures to 50 mg/m^3 $BaSO_4$ NPs aerosols. (**A**) A section of lymph node showing phagocytic cells with engulfed $BaSO_4$ nanoparticles (arrows) within phagolysosomes. (**B**) Higher magnification of boxed area in panel A showing abundant $BaSO_4$ particles in membrane-bound structures (arrows). (**C**) Higher magnification of boxed area in panel B showing $BaSO_4$ particles (arrows) within a phagocytic cell cytoplasm.

Concentration (mg/ml dH_2O)	d_H (nm)	PdI	ζ (mV)	Conductance (mS/cm)
0.67	222 ± 4	0.24 ± 0.01	−17.4 ± 1.9	0.02 ± 0.0
6.7	241 ± 5	0.37 ± 0.02	−18.6 ± 0.9	0.07 ± 0.01
33.3	388 ± 29	0.51 ± 0.08	−9.7 ± 0.6	0.15 ± 0.01

Table 3. Dynamic light scattering analysis of $BaSO_4$ NM-220 suspensions. Data are mean ± SD, n = 3. d_H, hydrodynamic diameter, PdI, polydispersity index, ζ, zeta potential.

Discussion

This study describes the fate of inhaled $BaSO_4$ NPs and the barium they contain from their initial lung deposition until their retention in the lungs and other organs in a rat model. We have previously reported that lung clearance of barium from $BaSO_4$ was far faster than cerium from CeO_2 NPs (9.6 vs. 140 days), despite $BaSO_4$ NPs having low dissolution rates in various simulant fluids[18,20]. The percentage of barium and cerium dissolved after 28-day incubation of $BaSO_4$ and CeO_2 NPs in phagolysosomal simulant fluid were 0.1% and <0.002% (lower than detection limit), respectively[18,20]. These data suggest that the dissolution rate of $BaSO_4$ is different from CeO_2 NPs in the lungs and that dissolution rates *in vivo* are different from those in cell-free simulant fluids. The present study sought to examine how much barium and in what forms are the barium retained in the lungs and selected organs (spleen, liver, bone, bone marrow and lymph nodes) after a 2-year inhalation exposure, and 4 weeks after IT

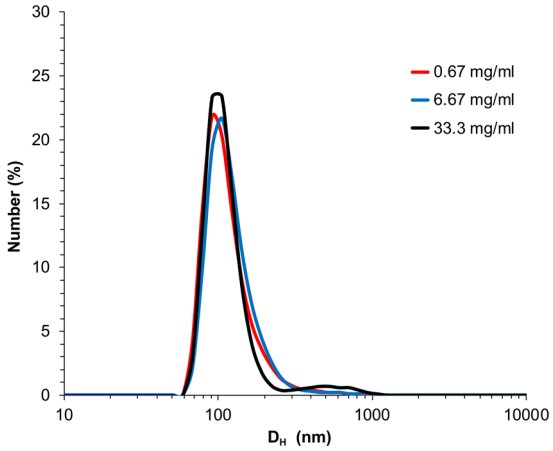

Figure 4. Study 2. Dynamic light scattering size distribution analyses of $BaSO_4$ nanoparticle suspensions in distilled water after sonication at 242 J/ml. Besides hydrodynamic diameters shown here, zeta potentials, polydispersity index and conductance were also measured (See Table 3).

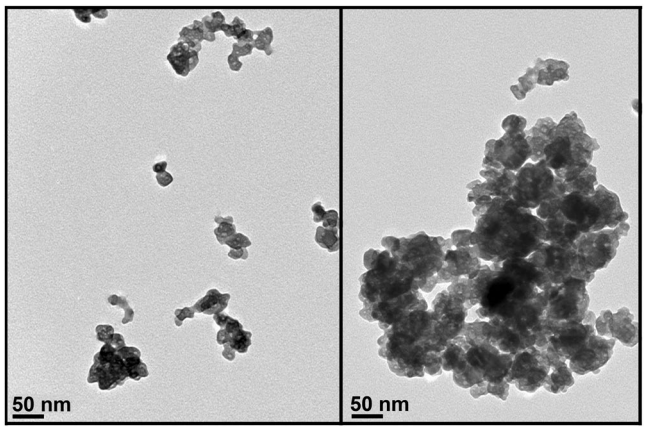

Figure 5. Study 2. TEM micrograph of sonicated suspension of 0.67 mg/ml $BaSO_4$ NPs in distilled water. Left panel shows individual particles (~25 nm) and small agglomerates. The right panel shows a bigger agglomerate of $BaSO_4$ nanoparticles seen in a more concentrated 33.3 mg/ml suspension.

instillation of $BaSO_4$ NPs. To determine the contribution of particle dissolution on barium translocation from the lungs, we also examined barium retention in the same organs after IT instillation of ionic Ba delivered as $BaCl_2$, a water-soluble salt of barium. *In toto*, our data suggest that the majority of barium from $BaSO_4$ NPs translocates from the lungs only after particle dissolution and ion transport to primarily the bone. A small fraction of $BaSO_4$ NPs translocate as intact particles to tracheobronchial but not to mesenteric lymph nodes.

After the final day of multiple inhalation exposure of rats in Study 1, the barium concentrations and estimated barium contents in the lungs, liver, lymph nodes, bone and bone marrow were measured. Based on these current data and on the previous reports in rats examined at 1, 28, and 90 days[18,28], we found that barium continuously accumulated in the lungs up to 360 days. No change in barium content was seen between 360 days and 2 years, suggesting that deposition equaled clearance rates. The highest concentrations of barium in the exposed animals were measured in the lungs and lymph nodes (tracheobronchial and mediastinal) followed by the hard bone and bone marrow. The liver had the lowest concentration. The highest amounts of barium were found in the lungs as expected and in hard bone, consistent with both our previous[18] and our current data from Study 2 in which rats were IT-instilled with the same batch of $BaSO_4$ NPs.

Our data indicate that lung clearance of $BaSO_4$ NPs becomes slower as lung burden increases, as reported in other studies[30,31]. Based on previous barium data from Study 1, the calculated lung clearance half-time from 90 days when the lung burden of barium was 1.6 mg/lung (1.24 mg/g lung weight) was approximately 56 days[28]. We have also shown that the lung burden after 28 days (0.84 mg/lung) decreased by 95% after 34 days[18]. Additionally, when deposited barium after IT instillation was 0.25 mg/lung (0.21 mg/g lung weight), the clearance half-time was shorter (9.5 days)[18]. Since no rats were continued after the end of the 2-year inhalation exposure, lung clearance when the retained barium was much higher could not be determined. The decreasing clearance with increasing lung barium burden increasing suggests that the clearance mechanisms, such as mucociliary clearance and NP dissolution in phagolysosomes, might have been impaired. However, we also observed that during the second

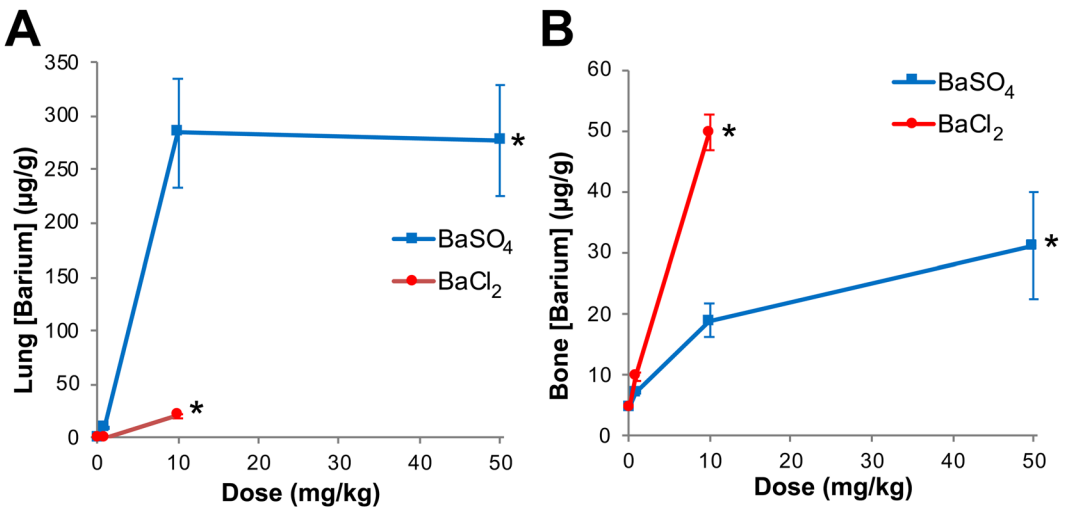

Figure 6. Study 2. Tissue concentrations of barium post-instillation of $BaSO_4$ NPs or $BaCl_2$ solution in rats. (**A**) Barium concentration in the lungs at 28 days post-instillation. There were significant dose-dependent increases in lung retention of barium post-instillation of $BaSO_4$ nanoparticles and $BaCl_2$ (*$P < 0.001$, ANOVA). Barium concentration in the lungs instilled with ionic barium ($BaCl_2$) was lower than with $BaSO_4$ NPs. (**B**) Barium concentration in bone (without bone marrow) at 28 days post-instillation. There were also dose-dependent increases in retained barium in bone (*$P < 0.001$, ANOVA). Significantly higher amounts of barium were retained in the bone of rats instilled with $BaCl_2$. The slopes of bone barium concentrations were significantly different between $BaCl_2$ and $BaSO_4$ animals ($P < 0.001$, ANOVA). n = 4–5 rats per group. Note: Doses are for mass of $BaSO_4$ NPs and $BaCl_2$, not of barium. The % Ba in $BaSO_4$ NPs and $BaCl_2$ are 58.8 and 65.9, respectively.

year of continuous exposure, barium in the lungs did not increase further (Fig. 1A), indicating that the rate of deposition was similar to the rate of lung clearance. This observation suggests that the barium was translocated from the lungs through pathways and mechanisms not previously understood. We believe particle dissolution leads to translocation of barium ions across the air-blood barrier followed by uptake by bone and other organs. Interestingly, substantial amounts of $BaSO_4$ particles translocated to the lymph nodes. Barium concentrations in the lymph nodes were found to be as high as in the lungs (Table 2).

The faster lung clearance of $BaSO_4$ compared to other poorly soluble particles such as CeO_2 and TiO_2 suggests that $BaSO_4$ solubility *in vivo* is substantially higher despite their similar poor solubility in cell-free simulant fluids. Indeed, dissolution rates *in vitro* simulated conditions are much slower than when particles are ingested by alveolar macrophages. It has been shown that dissolution rates of cobalt oxide particles were faster when taken up by human and canine alveolar macrophages *in vitro* than when these particles were incubated in cell-free media with simulated pulmonary conditions[32].

Is it possible that $BaSO_4$ NPs can more easily translocate as intact NPs through the air-blood barrier than CeO_2 NPs? Do the high amounts of barium in the bone prove translocation of intact $BaSO_4$ NPs from the lungs to the bone? To explore this possibility, we compared the biokinetics of barium post-instillation of $BaSO_4$ NPs versus barium ions ($BaCl_2$). We compared the barium concentrations in the lungs and bones of rats instilled with $BaSO_4$ NPs versus barium ions ($BaCl_2$ dissolved in water) at 28 days post-instillation. The amounts of barium remaining in the lungs increased with increasing mass dose of instilled $BaSO_4$ NPs. However, the lung barium concentrations were the same with 10 and 50 mg/kg doses. Greater amounts of barium translocated to tracheobronchial lymph nodes when rats were dosed with 50 mg/kg (Table 4), similar to rats in Study 1. Lung injury, inflammation, and increased fluid exiting the lungs via the lymphatics when a higher dose of barium was delivered in a single bolus might have enhanced the clearance of barium from the lungs.

Ionic barium was cleared almost completely from the lungs by 28 days. This suggests that once $BaSO_4$ NPs dissolve in the lungs, ionic barium can be translocated from the lungs to the circulation and other organs. Higher amounts of barium from $BaCl_2$ compared with $BaSO_4$ NPs were retained in the hard bone. These data indicate that the relatively higher bioavailability of barium after inhalation or instillation of $BaSO_4$ NPs is due to NP dissolution and subsequent transport of ionic barium from the lungs into extrapulmonary sites especially the bone, bone marrow and lymph nodes. It is unlikely due to the movement of intact NPs across tight epithelial barriers.

Transmission electron microscopy was used to look for intact $BaSO_4$ particles especially in tissues with high barium concentration. Whether IT-instilled or inhaled, the majority of retained $BaSO_4$ NPs in the lungs were seen as particles within phagolysosomes in alveolar macrophages and less commonly in type II epithelial cells and neutrophils. We observed $BaSO_4$ NPs within endosomes of phagocytic cells in tracheobronchial but not in the mesenteric lymph nodes despite their high barium concentrations. These particles could have reached these lymph nodes either as extracellular or more likely phagocytosed particles within macrophages from the lungs. Barium in mesenteric lymph nodes might have reached there as ionic barium from the tracheobronchial lymph nodes. The $BaSO_4$ NPs in the lungs of IT-instilled rats were densely packed within phagolysosomes and had a similar appearance as that of the original particle suspension. However, after chronic inhalation, the particles

Study 2		$BaSO_4$			$BaCl_2$		
Organ	Dose (mg/kg)	[Ba] µg/g	Organ Wt. (g)	Total Ba (µg)	[Ba] µg/g	Organ Wt. (g)	Total Ba (µg)
Lungs	0	0.01 ± 0.01#	1.10 ± 0.10	0.02 ± 0.02	0.01 ± 0.01#	1.10 ± 0.10	0.02 ± 0.02
	1	10.06 ± 0.61	1.17 ± 0.10	11.76 ± 0.57	0.21 ± 0.13*	1.30 ± 0.08	0.27 ± 0.17*
	10	284.6 ± 50.7	1.21 ± 0.09	344.4 ± 55.6	20.12 ± 1.87*	1.17 ± 0.13	23.4 ± 2.40*
	50	276.6 ± 51.5	1.30 ± 0.14	355.3 ± 17.0	N.D.		
Bone	0	4.71 ± 0.33#	16.8 ± 1.06	79.06 ± 6.85	4.71 ± 0.33#	16.8 ± 1.06	79.06 ± 6.85
	1	7.10 ± 0.27	18.3 ± 1.62	130.3 ± 12.9	9.74 ± 0.65	18.1 ± 0.76	176.3 ± 13.7*
	10	18.9 ± 2.75	18.1 ± 0.77	342.4 ± 48.8	49.78 ± 2.98*	17.2 ± 1.48	851.4 ± 31.1*
	50	31.2 ± 8.8	18.5 ± 1.87	562.5 ± 187.3	N.D.		
Bone Marrow	0	0.17 ± 0.19	10.7 ± 0.68	1.80 ± 1.85	0.17 ± 0.19	10.7 ± 0.68	1.80 ± 1.85
	1	0.07 ± 0.02	11.7 ± 1.03	0.81 ± 0.33	0.10 ± 0.02	11.6 ± 0.49	1.11 ± 0.22
	10	0.22 ± 0.05	11.6 ± 0.49	2.51 ± 0.61	0.24 ± 0.05	11.0 ± 0.95	2.63 ± 0.68
	50	0.24 ± 0.04	11.8 ± 1.20	2.83 ± 0.76	N.D.		
Liver	0	0.006 ± 0.004	11.1 ± 1.54	0.07 ± 0.05	0.006 ± 0.004	11.1 ± 1.54	0.07 ± 0.05
	1	0.005 ± 0.002	12.2 ± 1.86	0.06 ± 0.02	0.007 ± 0.002	11.3 ± 1.02	0.08 ± 0.03
	10	0.007 ± 0.005	11.7 ± 0.89	0.08 ± 0.07	0.007 ± 0.001	10.9 ± 1.19	0.08 ± 0.02
	50	0.008 ± 0.001	12.8 ± 2.74	0.10 ± 0.02			
Lymph Nodes	0	0.07 ± 0.03#	N.D.		0.07 ± 0.03	N.D.	
	1	0.31 ± 0.51	N.D.		0.09 ± 0.03	N.D.	
	10	5.89 ± 5.73	N.D.		0.11 ± 0.03	N.D.	
	50	41.38 ± 10.2	N.D.		N.D.		

Table 4. Barium concentration and content in selected tissues of rats 28 days after intratracheal instillation of 1, 10 or 50 mg/kg $BaSO_4$ nanoparticles and 1 or 10 mg/kg $BaCl_2$. Data are mean SD, n = 5 per group. Lymph nodes – tracheobronchial. Total bone and bone marrow weights were estimated as 5% and 3.2% of body weight, respectively. N.D., not determined, estimate of total lymph node mass in rats is not available. $BaCl_2$ at 50 mg/kg was highly toxic. *$P < 0.001$, Student's T test, $BaCl_2$ vs. $BaSO_4$. #$P < 0.001$, ANOVA. Dose-dependent increases. Note: Doses are for mass of $BaSO_4$ NPs and BCl_2, not of barium. The % Ba in $BaSO_4$ NPs and $BaCl_2$ are 58.8 and 65.9, respectively

were sparsely distributed, and the individual particles were less electron dense. These morphologic changes suggest gradual particle dissolution within the phagolysosomes over a period of months or more. Most of the $BaSO_4$ particles were taken up by alveolar macrophages at 7 days post-instillation, similar to our previous observation in BAL cells from the lungs of rats at 24 hours after instillation of $BaSO_4$ and CeO_2 NPs[33]. These data indicate that $BaSO_4$ NPs deposited in the lungs are readily phagocytosed by macrophages. No particles were seen in the bone marrow and liver, as well as in the lungs of air-exposed control and $BaCl_2$-instilled rat lungs. All these findings suggest that intact $BaSO_4$ NPs can translocate to anatomically close lymph nodes via the lymphatics. But few are likely to translocate into the circulation as free nanoparticles. Recent reports on other poorly soluble gold and CeO_2 NPs also conclude that NP translocation across the air-blood barrier is a rare event[20,33–35].

We also employed spectroscopic analysis of the same tissues using SRS microscopy to explore whether barium in multiple tissues was in the form of $BaSO_4$ or not. This technique is based on identifying the characteristic Raman shifts of $BaSO_4$ in unstained tissue sections. The lung, bone, liver, spleen and kidney of rats instilled with $BaSO_4$ NPs or ionic $BaCl_2$ were examined. The signature Raman shift of $BaSO_4$ was present in several foci in the lungs of rats instilled with $BaSO_4$ NPs but not with soluble $BaCl_2$. No signature Raman shift for $BaSO_4$ was found in the lungs, bone, liver, spleen or kidneys from uninstilled control, $BaCl_2$- and $BaSO_4$-instilled rats. Our findings from SRS further confirm that translocation of barium from $BaSO_4$ NPs to extrapulmonary organs is not as intact particles.

Conclusions

Our data indicate that barium translocates from the lungs after dissolution of $BaSO_4$ NPs within alveolar macrophages. This conclusion is supported by comparing lung and bone barium concentrations in $BaSO_4$ NP-instilled versus $BaCl_2$-instilled rats. Furthermore, we found no evidence of specific $BaSO_4$ Raman spectral characteristics in extrapulmonary organs. Thus, the abundant barium in bone and mesenteric lymph nodes must represent ionic barium's incorporation into the bone matrix as it forms and do not represent uptake of intact NPs. Electron microscopic imaging show that some intact $BaSO_4$ NPs are transported to lung-associated lymph nodes most likely via the lymphatic circulation, but not to distant (mesenteric) lymph nodes. Additionally, clearance of $BaSO_4$ NPs from the lungs is faster than can be predicted from its very low dissolution in simulant fluids. Thus, our data also underscore the limitations of *in vitro* dissolution assays in predicting biokinetics *in vivo* and emphasizes that solubility in water or lung simulant fluids needs to be carefully interpreted.

The precise mechanisms of how barium is transported from the phagolysosomes to the blood, and to extrapulmonary organs deserves further study. Additional analyses using high resolution transmission electron microscopy to study bioprocessing of $BaSO_4$ particles in the lungs, and the chemical/molecular forms of barium in the bone are underway.

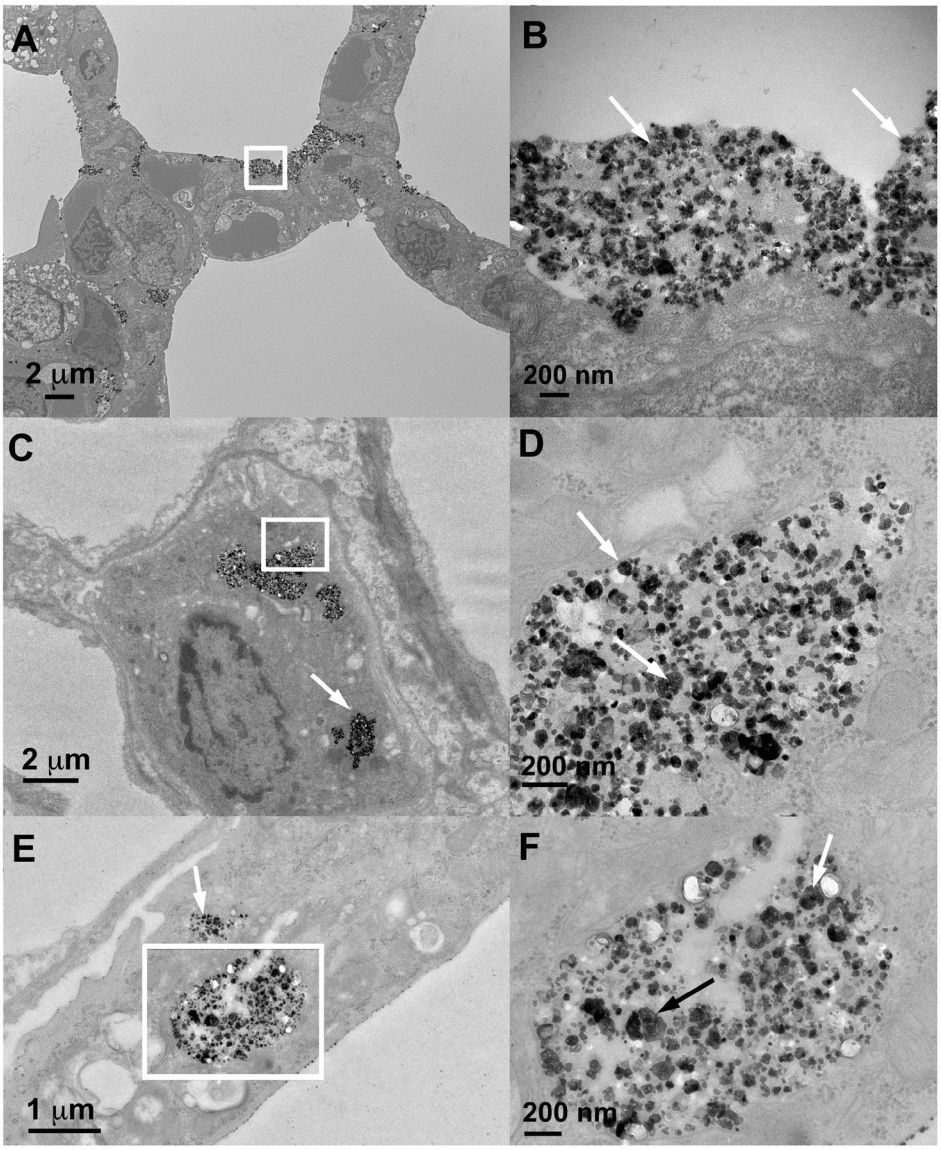

Figure 7. Study 2. Rat lung at 5 minutes (**A**,**B**) and 7 days (**C**–**F**) post-instillation of 10 mg/kg $BaSO_4$ NPs. (**A**) $BaSO_4$ NPs are shown lining the alveolar walls of rat lung immediately (5 minutes) post-instillation. The majority of $BaSO_4$ NPs were located extracellularly. (**B**) Higher magnification of boxed area in panel A showing $BaSO_4$ particles (arrows). (**C**) At 7 days post-instillation, alveolar macrophages with engulfed $BaSO_4$ nanoparticles (arrows) within phagolysosomes. (**D**) Higher magnification of boxed area in panel C showing $BaSO_4$ particles (arrows) in membrane-bound phagosomes. (**E**) Type II epithelial cell with internalized $BaSO_4$ nanoparticles (arrows). (**F**) Higher magnification of boxed area in panel E showing $BaSO_4$ particles (arrows) in membrane-bound vesicles in type 2 epithelial cell cytoplasm.

Methods

Characterization of $BaSO_4$ nanoparticles and $BaCl_2$. The $BaSO_4$ NPs (NM-220) used for these studies were a reference material prepared for the Nanomaterial Testing Sponsorship Program of the Organization for Economic Cooperation and Development (OECD). The characterization of the original batch distributed as NM-220 has been published[36]. Since Study 1 (2-year inhalation) requires large amounts, $BaSO_4$ NPs were reproduced at a different production plant using the same synthesis protocol. This reproduced batch was characterized by the same methods. Barium chloride anhydrous beads (99.99% pure) were obtained from Sigma-Aldrich (St. Louis, MO) and were used to prepare a stock solution of $BaCl_2$ at 50 mg/ml in distilled water.

Experimental Design: Study 1 - Two-year inhalation exposure of rats to aerosol of barium sulfate nanoparticles. The protocols for the long-term inhalation studies were approved by the local authorizing agency in Landesuntersuchungsamt, Koblenz, Germany. The procedures for inhalation exposure, aerosol generation and the monitoring system have been described[18]. Female Wistar Han rats were obtained at 7 weeks of age from Charles River Laboratories (Sulzfeld, Germany). The animals were maintained in groups of up to 5

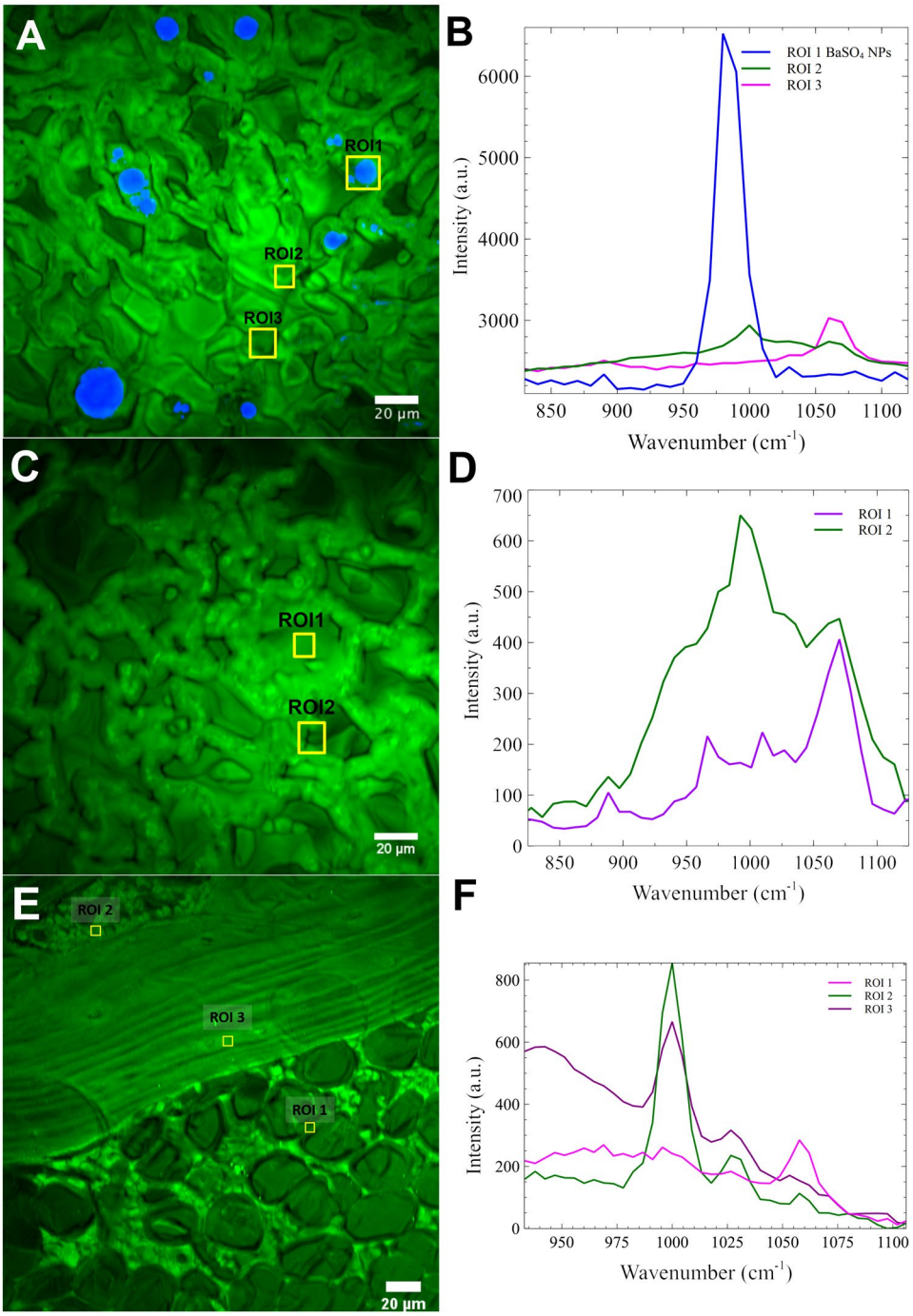

Figure 8. Study 2. Stimulated Raman spectroscopy microscopic examination of lungs and bone 28 days after IT instillation of 50 mg/kg $BaSO_4$ NPs. (**A**) Areas with characteristic Raman spectrum of $BaSO_4$ are shown in blue. (**B**) Raman spectra of three selected regions of interest (ROI) in panel A. Region of interest 1 (ROI 1) shows specific wavenumber for $BaSO_4$. ROI 2 and ROI 3 did not show characteristic wavenumber for $BaSO_4$. (**C**) Rat lung post- instillation of 10 mg/kg $BaCl_2$. (**D**) No specific Raman spectrum of $BaSO_4$ was detected in the lungs of rat instilled with $BaCl_2$ solution. ROI 1 and ROI 2 are shown. (**E**) Rat bone at 28 days post- instillation of 50 mg/kg $BaSO_4$ NPs. (**F**) No specific Raman spectrum of $BaSO_4$ was detected. Regions of interest (ROI) 1, 2 and 3 are shown. Examination of the lungs, spleen, liver and kidneys in uninstilled control and in rats instilled with $BaSO_4$ or $BaCl_2$ did not show specific Raman spectrum of $BaSO_4$ (data not shown).

animals in a polysulfon cages (TECNIPLAST, Germany) with access to wooden gnawing blocks, GLP certified feed (Kliba laboratory diet, Provimi Kliba SA, Kaiseraugst, Basel, Switzerland) and water *ad libitum*. Rats were exposed to 50 mg/m^3 $BaSO_4$ aerosol or filtered air for 24 months (6 h/day, 5 consecutive days/week). The animals were exposed while in wire cages located in a stainless-steel whole-body inhalation chamber (V = 2.8 m^3 or

$V = 1.4\ m^3$). The aerosols entered the inhalation chambers with the supply air and were removed by an exhaust air system with 20 air changes per hour. When containing control animals, the chamber air pressure was above the room air pressure to ensure that no room air reaches the control animals. For the $BaSO_4$-exposed rats, the chamber air pressure was negative to prevent contamination of the laboratory as a result of particle leakages from the inhalation chambers.

The majority of the cohort was used for histopathologic examination. One day after the last exposure, six rats (two air-exposed control and four $BaSO_4$-exposed) were euthanized and tissue samples were collected and processed. Samples of lung, liver, lymph nodes, bone and bone marrow from the six rats were collected and frozen. These were analyzed for barium concentration using ICP-MS. Parts of the same organs were processed for electron microscopy as described below.

Experimental Design: Study 2 - Intratracheal instillation of barium sulfate nanoparticles and barium chloride solution in rats. The protocols used in the instillation study were approved by the Harvard Medical Area Animal Care and Use Committee. Male Wistar Han rats (10 weeks old) were obtained from Charles River Laboratories (Wilmington, MA) and were housed in microisolator cages under controlled conditions of temperature, humidity, and light at the Harvard Center for Comparative Medicine. They were fed commercial chow (PicoLab Rodent Diet 5053, Framingham, MA) and reverse-osmosis purified water *ad libitum*. The animals were acclimatized in the facility for seven days before the start of experiments.

$BaSO_4$ NPs were suspended in sterile distilled water at 0, 0.67, 6.7 or 33.3 mg/ml for intratracheal instillation (IT) at doses of 0, 1, 10 and 50 mg/kg body weight, respectively. $BaCl_2$ was dissolved in sterile water at 0.67 and 6.7 mg/ml for 1 and 10 mg/kg doses, respectively. The volume dose was held constant at 1.5 ml/kg. Suspensions in tubes were sonicated with a Branson Sonifier S-450A (Branson Ultrasonics, Danbury, CT, USA) fitted with a cup sonicator at 242 J/ml, the critical dispersive energy shown to maximally disperse these particles in water[37] while immersed in running cold water to minimize heating of the particles. The hydrodynamic diameter (d_H), polydispersity index (PdI), conductance, and zeta potential (ζ) of each suspension were measured using a Zetasizer Nano-ZS (Malvern Instruments, Worcestershire, UK). Aliquots of each suspension were also examined under electron microscopy.

Each rat was weighed, and the volume dose of instilled particles was calculated. The NP suspension was loaded in a sterile syringe with attached blunt-tipped 18-gauge gavage needle. Each rat was then anesthetized with vaporized isoflurane (Piramal Healthcare, Bethlehem, PA), restrained on a slanted board, and held upright by their upper incisor teeth resting on a rubber band. The larynx was transilluminated with focused light for better visualization of the glottis during instillation. The tip of the needle was gently inserted into the trachea between the vocal cords, with the tip just above the tracheal bifurcation. The $BaSO_4$ NP suspension or $BaCl_2$ solution was gently delivered in one bolus.

Rats were humanely killed at 5 minutes (n = 2), 7 days (n = 2), and 28 days (n = 7) after dosing. Rats were anesthetized with vaporized isoflurane and euthanized by exsanguination via the abdominal aorta. The lungs, liver, tracheobronchial lymph nodes, bone marrow from the two femoral bones and femur (hard bone) were collected and placed in pre-weighed tubes. Barium concentration in each sample from 5 rats/group sacrificed at 28 days was measured using ICP-MS. Two rats euthanized at each of time points (7, 28 and 60 days) after instillation were used for morphologic examination of lungs, bone, spleen, liver and kidneys as described below.

Tissue analysis of barium content using ICP-MS. Tissue samples from selected organs in rats from Study 1 and Study 2 were analyzed for barium concentrations. In Study 1, barium concentration in the lungs, lymph nodes (tracheobronchial and mesenteric), liver, bone and bone marrow of $BaSO_4$ aerosol-exposed and air-exposed control rats were measured. In Study 2, barium concentration in the lungs, liver, tracheobronchial lymph nodes, bone marrow, and bone (without marrow) at 28 days post-instillation were measured. All samples were handled with special care to avoid contamination during processing. Samples were analyzed for barium by inductively coupled plasma mass spectrometry (ICP-MS) (Luna Nanotech, Ontario, ON, Canada). Tissue samples were digested with nitric acid for 24 h, and then further digested with hydrogen peroxide for 24 h at room temperature. Ultrapure water was used for final sample dilution.

Electron microscopic examination of lungs and other tissues. In Study 1, lung and other tissue samples from two control and four $BaSO_4$-exposed rats were collected and processed for electron microscopic examination. In Study 2, lungs from two rats per group were fixed in neutral buffered 10% formalin via the trachea at 30 cm water pressure. The bone, spleen, liver and kidneys were immersion-fixed in the same fixative. The fixed tissues were trimmed, paraffin embedded and sectioned. The sections were stained with hematoxylin and eosin. Lung, liver, spleen, kidney and decalcified bone sections were examined under light microscopy. Unstained paraffin-embedded tissue sections were examined using SRS microscopy.

Tissue samples from two rats per group from Study 2 euthanized at 5 minutes, and 7 and 28 days post-dosing were processed for electron microscopic examination of lung tissues. Each rat was anesthetized with vaporized isoflurane and were whole-body perfused with heparinized saline via the right ventricle, followed by 2.5% glutaraldehyde in HEPES buffer, pH 7. Fixed lungs were stored at 4 °C in the same fixative prior to processing and Epon embedding, sectioning and examination under electron microscopy.

Stimulated Raman scattering microscopy of lungs and other tissues. SRS microscopy is a nonlinear optical imaging technique that employs two ultrashort laser pulses (pump and Stokes) to coherently excite a Raman vibration that has an energy corresponding to the energy difference between the pump and the Stokes pulses. The coherent excitation improves signal intensity with much higher efficiency than spontaneous Raman and also eliminates interference from background fluorescence[38]. Therefore, it has advantages over spontaneous Raman as a useful non-destructive and label-free chemical imaging technique[39]. The tissue samples were analyzed

with an SRS microscope for the presence of spectral signature of $BaSO_4$ which has a Raman peak at 980 cm^{-1}. We imaged 5 random fields of view per slide to test for the presence of particulate $BaSO_4$ in each paraffin-embedded unstained tissue section. Several regions of interest (ROI) were analyzed for Raman spectra to differentiate $BaSO_4$-specific Raman peak from the surrounding tissue matrix. Additional details of SRS imaging protocols are provided in the Supplement.

Statistical analyses. Differences in organ concentrations of barium of rats in Study 1 and 2 were analyzed using Student t tests and analysis of variance (ANOVA) followed by Ryan-Einot-Gabriel-Welsch Multiple Range *post hoc* tests. Statistical analyses were performed using SAS statistical analysis software (SAS Institute, Cary, NC).

Ethical approval. Protocols for Study 1 were approved by the local authorizing agency in Landesuntersuchungsamt Koblenz, Germany. Animal experiments in Study 1 were performed following relevant OECD guidelines for Testing of Chemicals, Section 4: Health Effects, No. 453[38]. Animal experiments in Study 2 follow protocols in accordance with relevant guidelines and were approved by the Harvard Medical Area Animal Care and Use Committee (Boston, MA).

Data Availability

The datasets supporting the conclusion of this article are included within the article. There are 8 Figures and 4 Tables. All relevant raw data are freely available to researchers wishing to use them.

References

1. Maynard, A. D. & Kuempel, E. D. Airborne nanostructured particles and occupational health. *J Nanopart Res* **7**, 587–614 (2005).
2. Oberdorster, G. Toxicokinetics and effects of fibrous and nonfibrous particles. *Inhal Toxicol* **14**, 29–56, https://doi.org/10.1080/08958370175333862 2 (2002).
3. Cullen, R. T. *et al*. Inhalation of poorly soluble particles. I. Differences in inflammatory response and clearance during exposure. *Inhal Toxicol* **12**, 1089–1111, https://doi.org/10.1080/08958370050166787 (2000).
4. Shi, H., Magaye, R., Castranova, V. & Zhao, J. Titanium dioxide nanoparticles: a review of current toxicological data. *Part Fibre Toxicol* **10**, 15, https://doi.org/10.1186/1743-8977-10-15 (2013).
5. Choi, H. S. *et al*. Rapid translocation of nanoparticles from the lung airspaces to the body. *Nat Biotechnol* **28**, 1300–1303, https://doi.org/10.1038/nbt.1696 (2010).
6. Park, E.-J., Park, Y.-K. & Park, K. Acute toxicity and tissue distribution of cerium oxide nanoparticles by a single oral administration in rats. *Toxicol Res* **25**, 79–84 (2009).
7. Gomoll, A. H., Fitz, W., Scott, R. D., Thornhill, T. S. & Bellare, A. Nanoparticulate fillers improve the mechanical strength of bone cement. *Acta Orthop* **79**, 421–427, https://doi.org/10.1080/17453670710015349 (2008).
8. Mohn, D., Zehnder, M., Imfeld, T. & Stark, W. J. Radio-opaque nanosized bioactive glass for potential root canal application: evaluation of radiopacity, bioactivity and alkaline capacity. *Int Endod J* **43**, 210–217, https://doi.org/10.1111/j.1365-2591.2009.01660.x (2010).
9. Noreen, R. *et al*. Functional histology of glioma vasculature by FTIR imaging. *Anal Bioanal Chem* **401**, 795–801, https://doi.org/10.1007/s00216-011-5069-1 (2011).
10. Villalobos-Hernandez, J. R. & Muller-Goymann, C. C. Novel nanoparticulate carrier system based on carnauba wax and decyl oleate for the dispersion of inorganic sunscreens in aqueous media. *Eur J Pharm Biopharm* **60**, 113–122, https://doi.org/10.1016/j.ejpb.2004.11.002 (2005).
11. Aninwene, G. E. 2nd, Stout, D., Yang, Z. & Webster, T. J. Nano-$BaSO_4$: a novel antimicrobial additive to pellethane. *Int J Nanomed* **8**, 1197–1205, https://doi.org/10.2147/IJN.S40300 (2013).
12. Braakhuis, H. M., Park, M. V., Gosens, I., De Jong, W. H. & Cassee, F. R. Physicochemical characteristics of nanomaterials that affect pulmonary inflammation. *Part Fibre Toxicol* **11**, 18, https://doi.org/10.1186/1743-8977-11-18 (2014).
13. Buzea, C., Pacheco, I. I. & Robbie, K. Nanomaterials and nanoparticles: sources and toxicity. *Biointerphases* **2**, MR17–71 (2007).
14. Reijnders, L. The release of TiO2 and SiO2 nanoparticles from nanocomposites. *Polymer Degradation and Stability* **94**, 873–876 (2009).
15. Song, G. *et al*. A Low-Toxic Multifunctional Nanoplatform Based on Cu9S5@mSiO2 Core-Shell Nanocomposites: Combining Photothermal- and Chemotherapies with Infrared Thermal Imaging for Cancer Treatment. *Ad Func Mat*, https://doi.org/10.1002/adfm.201203317 (2013).
16. Stec, A. A. & Hull, T. R. In *Proceedings of the 5th International Seminar on Fire and Explosion Hazards, Edinburgh, UK, 23–27 April 2007*.
17. Dhawan, A., Sharma, V. & Parmar, D. Nanomaterials: A challenge for toxicologists. *Nanotoxicology* **3**, 1–9 (2008).
18. Konduru, N. *et al*. Biokinetics and effects of barium sulfate nanoparticles. *Part Fibre Toxicol* **11**, 55, https://doi.org/10.1186/s12989-014-0055-3 (2014).
19. Konduru, N. V. *et al*. Bioavailability, distribution and clearance of tracheally-instilled and gavaged uncoated or silica-coated zinc oxide nanoparticles. *Part Fibre Toxicol* **11**, 44, https://doi.org/10.1186/s12989-014-0044-6 (2014).
20. Molina, R. M. *et al*. Bioavailability, distribution and clearance of tracheally instilled, gavaged or injected cerium dioxide nanoparticles and ionic cerium. *Environ Sci: Nano*, https://doi.org/10.1039/c4en0034j (2014).
21. Roursgaard, M. *et al*. Time-response relationship of nano and micro particle induced lung inflammation. *Quartz as reference compound. Hum Exp Toxicol* **29**, 915–933, https://doi.org/10.1177/0960327110363329 (2010).
22. Braakhuis, H. M. *et al*. Particle size dependent deposition and pulmonary inflammation after short-term inhalation of silver nanoparticles. *Part Fibre Toxicol* **11**, 49, https://doi.org/10.1186/s12989-014-0049-1 (2014).
23. Seiffert, J. *et al*. Pulmonary toxicity of instilled silver nanoparticles: influence of size, coating and rat strain. *PLoS One* **10**, e0119726, https://doi.org/10.1371/journal.pone.0119726 (2015).
24. Cember, H., Hatch, T. F., Watson, J. A., Grucci, T. & Bell, P. The elimination of radioactive barium sulfate particles from the lung. *AMA Arch Ind Health* **13**, 170–176 (1956).
25. Cember, H., Watson, J. A. & Novak, M. E. The influence of radioactivity and lung burden on the pulmonary clearance rate of barium sulfate. *Am Ind Hyg Assoc J* **22**, 27–32, https://doi.org/10.1080/00028896109344129 (1961).
26. Cordelli, E. *et al*. No genotoxicity in rat blood cells upon 3- or 6-month inhalation exposure to CeO2 or BaSO4 nanomaterials. *Mutagenesis* **32**, 13–22, https://doi.org/10.1093/mutage/gew005 (2017).
27. Landsiedel, R. *et al*. Application of short-term inhalation studies to assess the inhalation toxicity of nanomaterials. *Part Fibre Toxicol* **11**, 16, https://doi.org/10.1186/1743-8977-11-16 (2014).
28. Schwotzer, D. *et al*. Effects from a 90-day inhalation toxicity study with cerium oxide and barium sulfate nanoparticles in rats. *Part Fibre Toxicol* **14**, 23, https://doi.org/10.1186/s12989-017-0204-6 (2017).

29. Brown, R. P., Delp, M. D., Lindstedt, S. L., Rhomberg, L. R. & Beliles, R. P. Physiological parameter values for physiologically based pharmacokinetic models. *Toxicol Ind Health* **13**, 407–484 (1997).
30. Yu, R. & Rappaport, S. Relation between pulmonary clearance and particle burden: a Michaelis-Menten-like kinetic model. *Occ Ennviron Med* **53**, 567–572 (1996).
31. Klosterkotter, W. & Bunemann, G. In *Inhaled particleds and vapors*. (ed. Davis, C. N.) 327–337 (Pergamon Press, 1961).
32. Kreyling, W. G., Godleski, J. J., Kariya, S. T., Rose, R. M. & Brain, J. D. *In vitro* dissolution of uniform cobalt oxide particles by human and canine alveolar macrophages. *Am J Respir Cell Mol Biol* **2**, 413–422, https://doi.org/10.1165/ajrcmb/2.5.413 (1990).
33. Konduru, N. V. *et al*. Protein corona: implications for nanoparticle interactions with pulmonary cells. *Part Fibre Toxicol* **14**, 42, https://doi.org/10.1186/s12989-017-0223-3 (2017).
34. Kreyling, W. G. *et al*. Air-blood barrier translocation of tracheally instilled gold nanoparticles inversely depends on particle size. *ACS Nano* **8**, 222–233, https://doi.org/10.1021/nn403256v (2014).
35. Schleh, C. *et al*. Biodistribution of inhaled gold nanoparticles in mice and the influence of surfactant protein D. *J Aerosol Med Pulm Drug Deliv* **26**, 24–30, https://doi.org/10.1089/jamp.2011.0951 (2013).
36. Wohlleben, W. *et al*. Nanospecific guidance in REACH: A comparative physical-chemical characterization of 15 materials with methodical correlations. *J. Ceram. Sci. Tech* **4**, 93–104 (2013).
37. Cohen, J., Deloid, G., Pyrgiotakis, G. & Demokritou, P. Interactions of engineered nanomaterials in physiological media and implications for *in vitro* dosimetry. *Nanotoxicology* **7**, 417–431, https://doi.org/10.3109/17435390.2012.666576 (2013).
38. Cheng, J. X. Coherent anti-Stokes Raman scattering microscopy. *Appl Spectrosc* **61**, 197–208, https://doi.org/10.1366/000370207781746044 (2007).
39. Cheng, J. X. & Xie, X. S. Vibrational spectroscopic imaging of living systems: An emerging platform for biology and medicine. *Science* **350**, aaa8870, https://doi.org/10.1126/science.aaa8870 (2015).

Acknowledgements

This study was funded by a grant from Cefic/LRI (European Chemical Industry Council Long Range Research Initiative) (Ludwigshafen, Germany) and by the National Institute of Environmental Health Sciences (ES000002). NVK was supported by a Pathway to Independence Award K99 5K99ES025813-02 from the National Institutes of Health. PQ received support from the Science Without Borders Program of Brazil administered by CAPES, the Brazilian Coordinating Office for the Advancement of Higher Education. We thank Thomas Donaghey, Leonardo Pipek, and Johnatan Gonçalves for their technical help, and Melissa Curran for her editorial assistance.

Author Contributions

R.M.M., N.V.K. and J.D.B. designed, performed and evaluated data from the experiments. P.Q. performed the *in vivo* instillation experiments. L.M.-H., S.G. and D.S. performed some aspects of experiments in Study 1. B.F. and D.F. performed the SRS microscopy. R.M.M., N.V.K. and J.D.B. drafted the manuscript. All authors read, revised and approved the manuscript.

Additional Information

Supplementary information accompanies this paper at https://doi.org/10.1038/s41598-019-44551-2.

Competing Interests: S.G. and L.M.-H. are employed at BASF S.E., a company that produces and markets nanomaterials. All other authors declare that they have no competing interests.

Publisher's note: Springer Nature remains neutral with regard to jurisdictional claims in published maps and institutional affiliations.